

# Scale-Variant Robust Kernel Optimization for Non-linear Least Squares Problems

SHOUNAK DAS

Department of Mechanical and Aerospace Engineering, West Virginia University, Morgantown, USA

JASON N. GROSS

Department of Mechanical and Aerospace Engineering, West Virginia University, Morgantown, USA

**Abstract**— In this article, we consider the benefit of increasing adaptivity of an existing robust estimation algorithm by learning two parameters to better fit the residual distribution. Our method uses these two parameters to calculate weights for Iterative Reweighted Least Squares (IRLS). This adaptive nature of the weights can be helpful in situations where the noise level varies in the measurements. We test our algorithm first on the point cloud registration problem with synthetic data sets and lidar odometry with open source real-world data sets. We show that the existing approach needs an additional manual tuning of a residual scale parameter which our method directly learns from data and has similar or better performance.

**Index Terms**— in Robust estimation, point cloud registration, adaptive loss, iterative non-linear least squares

## I. Introduction

Robustness is a very important property that is necessary for any estimation algorithm running on robotic systems. In real-world scenarios, noise levels fluctuate and sensor data gets corrupted by outliers (e.g., multipath reflections and jamming attacks in GNSS [1], presence of

Manuscript received XXXXX 00, 0000; revised XXXXX 00, 0000; accepted XXXXX 00, 0000.

This paragraph of the first footnote will contain the date on which you submitted your paper for review, which is populated by IEEE. This research was sponsored in part by the Alpha Foundation for the Improvement of Mine Safety and Health, Inc. (ALPHA FOUNDATION). The views, opinions, and recommendations expressed herein are solely those of the authors and do not imply any endorsement by the ALPHA FOUNDATION, its Directors and staff. This research was supported in part by USDA Grant #2022-67021-36124

Authors' addresses: S. Das and J. N. Gross are with the Department of Mechanical and Aerospace Engineering, West Virginia University, Morgantown, WV 26506 USA, E-mail: (sd0111@mix.wvu.edu; jason.gross@mail.wvu.edu); (*Corresponding author: Shounak Das*).

Mentions of supplemental materials and animal/human rights statements can be included here.

Color versions of one or more of the figures in this article are available online at <http://ieeexplore.ieee.org>.

0018-9251 © IEEE

wrong correspondences or dynamic objects in registration problems [2], slippage in wheel odometry data [3], dark or shaded areas in visual odometry). Current state-of-the-art methods try to detect these harmful scenarios and can either remove [4] or de-weight the suspected “bad” measurements [5]. In this article, the focus is on the de-weighting approach. First, we overview the literature and provide a description of previous works from which the proposed approach draws inspiration. Next, the proposed algorithm is described along with the intuition behind it. Lastly, this method is compared with other well-known approaches with respect to estimation performance using both synthetic data and real-world scenarios.

## II. Literature Review

Robust estimation aims at estimating the correct parameters with or without the presence of measurements errors that vary from the expected distribution (i.e., typically assumed Gaussian). Many of the modern robust estimation techniques used in robotics draw inspiration from works of Huber [6], Tukey [7], Hampel [8] in the field of robust statistics. Bosse et al. [9] gives concise descriptions of these statistical concepts called M-estimators and their applications to robotics. The importance of M-estimators in point cloud registration and visual navigation have been discussed in [10] [11]. The proposed algorithm uses a generalized version of these M-estimators developed by Barron [12] and extended by Chebrolu [2]. M-estimators fall within the de-weighting group of methods, which don't directly remove measurements. The intuition behind this is that, instead of assuming a Gaussian distribution for the measurement noise, these M-estimators have heavier tails, which solve for the parameters that best fit the overall data. An interesting connection between M-estimators and elliptical distributions was shown in [13], which was used for parameter estimation. The cost functions obtained from negative log-likelihood of these distributions are modified versions of the squared loss function, which are optimized to get to the correct solution. Some of these functions are non-convex and suffer from the local minima problem (eg. Redescending M-estimators). To tackle this, [5] uses the concepts of graduated non-convexity, along with the Black-Rangarajan duality [14], to devise an iterative algorithm for robust perception. Another common area of application for robust estimation is loop closures. To mitigate the effect of false loop closures, several researchers have considered approaches for adding robustness in the back in for SLAM application. Sunderhauf et al. [15] added binary scalars, or Switch Constrains, to measurements allowing them to be turned on/off in the optimization. Dynamic Covariance Scaling was then developed to give same theoretical benefit in a more efficient manner [16]. These methods were used for robust GNSS positioning in a factor graph framework in [17]–[19]. Recently AEROS [20] modelled all loop closures using robust cost functions with a single adaptive parameter and improved back end optimization.

The other group of the robust estimation methods focus on the finding the maximum number of measurements that satisfy a specific inlier condition, which is also called the Maximum Consensus (MC) problem [21]. One of the most well-known methods to solve these kind of problems is called Random Sample Consensus (RANSAC) [22]. Numerous variations of this algorithms have been developed [23], and still remains an important area of research. Antonante et al. [24] provides in-depth discussion of various robust estimation methods across different disciplines along with their computational limits. They develop minimally tuned algorithms that can tolerate large number of outliers. Shi et al. [4] uses invariance relations between measurements to solve MC problems by converting it into a maximal clique problem. Loop closures for multi-robot systems has been similarly modelled as a maximal clique problem analysed in [25].

We chose the de-weighting direction because of the effectiveness of robust cost functions for point cloud registration problems shown in several studies [26] [12] [5] [10] [2]. They are also easy to implement inside a non-linear least squares framework whereas the MC approaches are usually implemented as pre-processing step before the nonlinear least squares. Lastly, robust cost functions have been implemented in many state of the art lidar-SLAM packages like [27] [28] [29].

### III. M-estimators and least-squares

M-estimation [9] replaces the standard squared loss function by a function which reduces the effect of measurements with large residuals. This is a continuous optimization problem, which can be solved iteratively with gradient descent.

$$\theta^* = \underset{\theta}{\operatorname{argmin}} \sum_{i=1}^N \rho(x_i(\theta)). \quad (1)$$

Equation 1 can be solved by looking at how general (un-weighted or weighted) nonlinear least square problems are solved.

$$\hat{\theta} = \underset{\theta}{\operatorname{argmin}} \sum_{i=1}^N \|\mathbf{x}_i(\theta)\|^2.$$

$$\hat{\theta}_w = \underset{\theta}{\operatorname{argmin}} \sum_{i=1}^N w_i \|\mathbf{x}_i(\theta)\|^2.$$

Two families of methods are used generally: line search methods, such as Gauss-Newton, and trust region methods, such as Levenberg-Marquardt, both of which are iterative descent methods [30] [31]. Partially differentiating the least squares and M-estimation expressions in their scalar forms with respect to the unknown parameter  $\theta$  shows

$$\frac{1}{2} \frac{\partial (w_i x_i^2(\theta))}{\partial \theta} = w_i x_i(\theta) \frac{\partial x_i(\theta)}{\partial \theta}$$

$$\frac{\partial (\rho(x_i(\theta)))}{\partial \theta} = \rho'(x_i(\theta)) \frac{\partial x_i(\theta)}{\partial \theta}.$$

Comparing these two expressions, it is apparent that M-estimation can be solved exactly like a weighted nonlinear least squares problem. The weights in this case is given by

$$w_i = \frac{\rho'(x_i(\theta))}{x_i(\theta)}. \quad (2)$$

Hence this method of solving M-estimation problems is called Iterative Re-weighted Least Squares (IRLS) [9].

### IV. One function for all

In this paper, the approach we propose starts with Barron's work on unifying different robust cost functions [12].

$$\rho(x, \alpha, c) = \begin{cases} \frac{1}{2}(x/c)^2 & \text{if } \alpha = 2 \\ \log\left(\frac{1}{2}(x/c)^2 + 1\right) & \text{if } \alpha = 0 \\ 1 - \exp\left(-\frac{1}{2}(x/c)^2\right) & \text{if } \alpha = -\infty \\ \frac{|\alpha-2|}{\alpha} \left( \left( \frac{(x/c)^2}{|\alpha-2|} + 1 \right)^{\alpha/2} - 1 \right) & \text{otherwise} \end{cases} \quad (3)$$

This form of cost function is convenient because different variations of M-estimators can be expressed by changing the parameter  $\alpha$ .  $x$  is the residual value depending on the estimation problem at hand.  $c$  is sometimes referred to as the scale parameter. This article aims to understand the effects of changing  $\alpha$  and  $c$  values in different robust estimation scenarios. As described earlier, M-estimators de-weight suspected outlier residuals instead of removing them completely. This is helpful in cases where removing data can affect the solution accuracy such as GNSS estimation with a low number of available observations, or visual odometry in environments with limited feature. The weight depends on the derivative  $\frac{\partial \rho}{\partial x}$  and the residual  $x$ . The partial derivatives of this cost function with respect to  $x$  is given in Eq. 4.

$$\frac{\partial \rho}{\partial x}(x, \alpha, c) = \begin{cases} \frac{x}{c^2} & \text{if } \alpha = 2 \\ \frac{2x}{x^2+2c^2} & \text{if } \alpha = 0 \\ \frac{x}{c^2} \exp\left(-\frac{1}{2}(x/c)^2\right) & \text{if } \alpha = -\infty \\ \frac{x}{c^2} \left( \frac{(x/c)^2}{|\alpha-2|} + 1 \right)^{(\alpha/2-1)} & \text{otherwise} \end{cases} \quad (4)$$

The sum of cost of the all residuals can be optimized to solve for the unknown state

$$\hat{X} = \underset{\theta, \alpha, c}{\operatorname{argmin}} \sum_i \rho(x_i(\theta), \alpha, c). \quad (5)$$

A better understanding of the optimization problem can be obtained by looking at the partial derivatives of  $\rho$  with respect to  $\alpha$ .

$$\frac{\partial \rho}{\partial \alpha}(x, \alpha, c) \geq 0 \quad (6)$$

Since  $\rho$  in equation 3 is even with respect to  $c$ , only positive values for  $c$  are used. Equation 6 shows the cost decreases with decreasing  $\alpha$  when  $c$  is constant. Fig. 1 shows probability density as a function of  $\alpha$  and  $c$ . The problem of optimizing equation 5 with respect to  $(x, \alpha)$

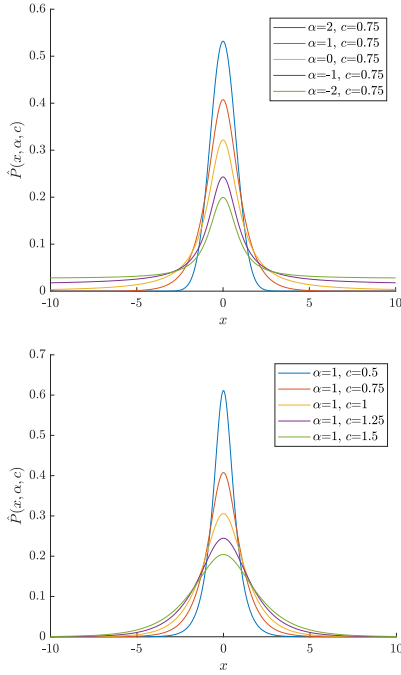


Fig. 1: Top :Probability density function for constant  $c$  and changing  $\alpha$ ,  
Bottom :Probability density function for constant  $\alpha$  and changing  $c$

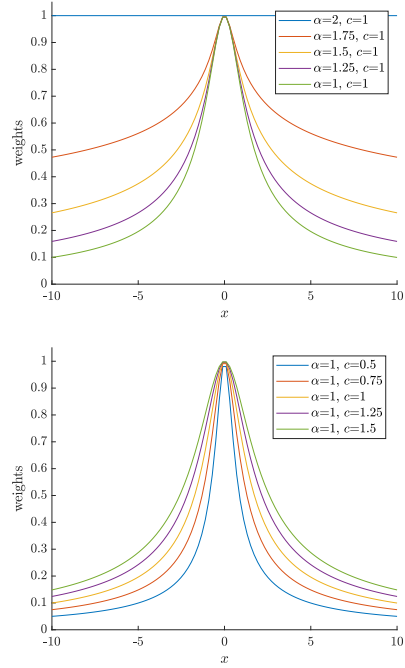


Fig. 2: Top : weights  $\frac{\rho'(x, \alpha, c)}{x}$  for constant  $c$  changing  $\alpha$ , Bottom :  
weights  $\frac{\rho'(x, \alpha, c)}{x}$  for constant  $\alpha$  changing  $c$

is that the solution will trivially move towards lower values of  $\alpha$ , thus not representing the true distribution of the residuals and, in turn, affecting the estimates of the unknown parameters. Barron et al. [12] removes this issue by assuming a distribution given by

$$P_*(x, \alpha, c) = \frac{1}{cZ(\alpha)} e^{-\rho(x, \alpha, c)} \quad (7)$$

$$Z(\alpha) = \int_{-\infty}^{\infty} e^{-\rho(x, \alpha, 1)} dx.$$

This creates a shifted version of cost function. Using negative log-likelihood we get

$$\rho_*(x, \alpha, c) = \rho(x, \alpha, c) + \log(cZ(\alpha)). \quad (8)$$

With this, whenever  $\rho_*$  is optimized with respect to  $(x, \alpha)$ , the solution cannot trivially go to the least value of  $\alpha$  due to the newly added penalty term. The optimization process attempts to balance between the lower cost of larger residuals and the higher cost of the inliers. However, another problem arises with this shifted expression, which is that  $Z(\alpha)$  is unbounded for negative values of  $\alpha$ . Thus the optimization cannot be done in the negative domain of  $\alpha$ , which is not ideal because negative  $\alpha$  values can be useful in presence of large residuals. Chebroly et al. [2] used a truncated version of  $Z(\alpha)$  to circumvent this issue

$$\hat{Z}(\alpha) = \int_{-\tau}^{\tau} e^{-\rho(x, \alpha, 1)} dx. \quad (9)$$

$\hat{Z}(\alpha)$  can be calculated for both positive and negative values of  $\alpha$ . The only assumption with this formulation is that any residual with magnitude greater than  $\tau$  has zero probability. Replacing  $Z(\alpha)$  with  $\hat{Z}(\alpha)$ ,  $P_*$  is obtained.

Instead of jointly optimizing over  $(x, \alpha, c)$ , [2] first finds the  $\alpha$  that has the lowest negative log-likelihood with the current residuals, and then solves equation 5 with iterative re-weighted least squares with this last optimal value of  $\alpha$ . These two steps are repeated until convergence is achieved.  $c$  is kept constant in this method and depends on the inlier measurement noise. The algorithm is described in 1.  $\theta$  is the vector of parameters to be estimated. This algorithm is referred to in this work as RKO.

---

#### Algorithm 1 Robust Kernel Optimization (RKO) [2]

---

```

Initialize  $\theta^0, \alpha^0, c$ 
while !converged do
  Step 1: Minimize for  $\alpha$ 
   $\alpha^t = \operatorname{argmin}_{\alpha} - \sum_{i=1}^N \log P_*(x_i(\theta^{t-1}), \alpha^{t-1}, c)$ 
  Step 2: Minimize robust loss using IRLS
   $\theta^t = \operatorname{argmin}_{\theta} \sum_{i=1}^N \rho(x_i(\theta), \alpha^t, c)$ 
end while

```

---

## V. Scale-variant Robust Kernel Optimization

Algorithm 1 has been shown to work well for LiDAR Simultaneous Localization and Mapping (SLAM) in the presence of dynamic objects as well as bundle adjustment [2]. However, manually setting the scale parameter  $c$  is difficult and is often done by trial and error. In this work, finding a way to learn  $c$  along with  $x, \alpha$  is considered for the purpose of yielding further improvements in

such situations. To that end, a slightly different variation of the probability distribution  $\hat{P}$  is proposed.

$$\begin{aligned}\hat{P}(x, \alpha, c) &= \frac{1}{\hat{Z}(\alpha, c)} e^{-\rho(x, \alpha, c)} \\ \hat{Z}(\alpha, c) &= \int_{-\tau}^{\tau} e^{-\rho(x, \alpha, c)} dx.\end{aligned}\quad (10)$$

Similar to the shifted cost above, the cost corresponding to this distribution is obtained by taking the negative log-likelihood

$$\hat{\rho}(x, \alpha, c) = \rho(x, \alpha, c) + \log(\hat{Z}(\alpha, c)). \quad (11)$$

The behavior of this probability distribution can be understood by looking at Fig. 1. In the top graph  $\hat{P}$  shows behavior similar to the  $P_*$ , where in the presence of large noise or outliers,  $\alpha$  decreases and thus creates a heavier-tailed distribution, with probability mass moving from the smaller residuals towards the larger residuals. Changing  $\alpha$  moves probability mass mostly between large and low residuals with less change in the mid residual range. This is where the increased adaptivity of  $\hat{P}$  over  $P_*$  can be understood. The right graph in Fig. 1 shows varying  $c$  with a constant  $\alpha$  moves probability mass between smaller residuals and mid-range residuals and minimal change in probability for larger magnitudes. Essentially, optimizing  $\hat{P}$  gives an additional “degree of freedom” of better fitting the existing residuals by adapting  $c$  along with  $\alpha$ . From a weight perspective, increasing and decreasing  $c$  results in a smoother and sharper drop in the weights respectively as residuals increase (Fig 2). Thus, with the addition of changing  $c$ , the optimization explores more values in the weight space which helps the IRLS step. Note for  $\alpha = 2$ , changing  $c$  does not change the weights, they all remain 1 (eq. 2). This is because  $c$  only affects the variance for the Gaussian distribution. Also  $\hat{P}(x, \alpha, c)$  being a probability density function can assume values larger than 1 which is the case when  $c$  takes lower values. Lower values of  $c$  help fit tighter residuals which is something RKO cannot do when  $c$  is fixed.

Now, given Algorithm 1, another step can easily be added in this method, where, after minimizing the negative log-likelihood with respect to  $\alpha$ , the negative log-likelihood with respect to  $c$  is minimized. We call this the Scale-variant Robust Kernel Optimization (S-RKO) method. The steps of this algorithm are shown in the proposed Algorithm 2. It is very similar to the original algorithm. It starts with initial guesses  $\theta^0$ ,  $\alpha^0$  and  $c^0$ . Then, for any time step  $t$ , the following steps are conducted: first, with the current value of  $c^{t-1}$ , and the residuals  $x(\theta^{t-1})$ , find  $\alpha^t$  that minimizes the negative log-likelihood of the residuals. This can be done easily with grid search. Next,  $c^t$  is obtained similarly by minimizing the negative log-likelihood that is calculated with  $x(\theta^{t-1})$  and  $\alpha^t$ . Note, ideally this search needs to be done over a 2D grid but we approximate this with learning best  $\alpha$  and  $c$  separately for reducing computational cost. Lastly, with  $\alpha^t$  and  $c^t$ , the loss function in equation 5 can be optimized iteratively using Gauss-Newton method. In steps 1 and 2

of this algorithm, in order to search for optimum values of  $\alpha$  and  $c$  we discretize over their possible ranges. A pre-computed table of values of  $\hat{Z}(\alpha, c)$  is used for each of the grid searches.

---

**Algorithm 2** Scale-variant Robust Kernel Optimization (S-RKO)

---

```
Initialize  $\theta^0, \alpha^0, c^0$ 
while !converged do
  Step 1: Minimize for  $\alpha$ 
   $\alpha^t = \operatorname{argmin}_{\alpha} - \sum_{i=1}^N \log \hat{P}(x_i(\theta^{t-1}), \alpha, c^{t-1})$ 
  Step 2: Minimize for  $c$ 
   $c^t = \operatorname{argmin}_c - \sum_{i=1}^N \log \hat{P}(x_i(\theta^{t-1}), \alpha^t, c)$ 
  Step 3: Minimize robust loss using IRLS
   $\theta^t = \operatorname{argmin}_{\theta} \sum_{i=1}^N \rho(x_i(\theta), \alpha^t, c^t)$ 
end while
```

---

## VI. Experiments

We test the proposed SRKO algorithm on point cloud registration with synthetic data and lidar odometry with real world data sets and compare performance with other robust methods from literature.

### A. Synthetic Data

The proposed algorithm, SRKO, is tested for the problem of pairwise point cloud registration problem with the open source implementation and synthetic range data sets provided in [26]. The registration algorithm of [26], referred to in the article as FastReg, rewrites the scaled Geman-McClure estimator as an outlier process using Black-Rangarajan duality [14] and solves it iteratively. Since this cost function is non-convex, to avoid local minima, the method starts with a convex version of this function and changes the scale parameter after every few iterations to increase the non-convexity. We refer the readers to [26] for details about these data sets which come from AIM@SHAPE repository, the Berkeley Angel dataset and the Stanford 3D Scanning repository. For these data sets, we compare performances of fixed Huber, RKO, SRKO and FastReg. Similar to [26], we use two versions of the 25 point clouds. One is a clean version with no noise and another one is noisy version with added Gaussian noise of  $\sigma = 0.005$ . Target point clouds are generated with truth transformation for proper evaluation. Both source and target point clouds have been normalised with respect to a diameter of their surface. Correspondences between the source and target point clouds are obtained by matching Fast Point Feature Histogram (FPFH) features [32]. The registration is done by minimizing the point to point distance between correspondences using Gauss-Newton method. Note the only difference between the methods that are being compared is the way the residuals are weighted in IRLS. For completeness, we also

show the Huber and Geman McClure weight formulas here :

$$w_{huber}(x, c) = \begin{cases} 1 & |x| \leq c \\ \frac{c}{|x|} & |x| > c \end{cases} \quad (12)$$

$$w_{geman}(x, \mu) = \frac{\mu^2}{(\mu + x^2)^2} \quad (13)$$

## B. Real world data

We also test Huber, RKO, SRKO and FastReg with the lidar inertial odometry SLAM package LIO-SAM [33]. Due to lack of GPS data, for evaluation, we compare performance of the above 4 methods without loop-closures with respect to loop-closure assisted standard LIO-SAM as a reference. The open-source implementation provided by the authors of [33] use a weight function of the form  $1 - 0.9|x|$  where  $x$  is the distance between an edge feature and its corresponding edge in the map (Eq. 10 in [33]) or the distance between a planar feature to its corresponding plane along the plane normal in the map. They also remove residuals which are larger than a certain residual threshold. In our implementations of the 4 methods, we allow all residuals and let the robust methods de-weight suspected outliers. We consider the open-source implementation as reference solution. We evaluate on the *park*, *garden*, *rotation* and *campus* data sets provided in [33].

## VII. Results and Discussion

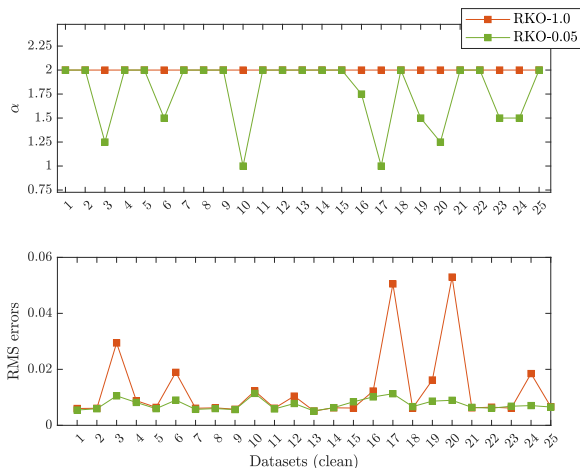


Fig. 3: Effect of residual scaling in RKO

For the synthetic algorithm implementations of RKO and SRKO,  $\hat{Z}(\alpha, c)$  are calculated with  $\tau$  values set to 10, meaning it is assumed that there are no residuals with magnitude greater than 10. For Huber kernel, we set the scale parameter value to 1.3 which is a common choice [6]. For RKO,  $c$  is fixed to 1 and  $\alpha$  has a discretized range of  $[-4 : 0.25 : 2]$ . For SRKO, we first test with  $c$

values greater than or equal to 1. The range of discretized  $c$  values tested for this case are  $[1 : 0.25 : 3]$ . The residual used here is the point to point distance between correspondences. The initialization point for both RKO and SRKO is  $(\alpha, c) = (2, 1)$ , which is the standard Gaussian distribution.

When tested with 25 clean and noisy data sets, we found the performances of Huber, RKO and SRKO to be worse than FastReg. Next, we tried scaling the residuals before learning by  $s$ . That is, instead of  $x$ , we learn the distribution of  $\frac{x}{s}$ . The scale values we tested with are 0.1 and 0.05. Interestingly, we found that lowering the scales resulted in  $\approx 2x$  improvement in performance for both clean and noisy data (Tables I, II). The learned  $\alpha$  values are similar for both RKO and SRKO, and the learned  $c$  values of SRKO mostly stay at 1.

The motivation for residual scaling can be understood from the Figure 3. The top plot shows the learned  $\alpha$  and the bottom one shows the registration performances for scales 1 and 0.05. Scale 0.05 case improves performance in data sets for which learned  $\alpha$  lower than 2. This points to the fact that scale 1 is under-fitting the residuals with  $\alpha = 2$  resulting in equal weights for all residuals. For scale 0.05, RKO learns a more robust  $\alpha$  which de-weights the larger residuals. This happens because the un-scaled residual values for these data sets lie close to 0 (Fig 4 top). This results in RKO weighting them equally. However, just being close to zero does not guarantee that residual to be an inlier, since the true scale is unknown. Scaling with 0.05 increases the residual by a factor of 20 which helps RKO find a better fit with a more robust  $\alpha$  and de-weights the larger residuals. The same thing happens for Huber kernel where all un-scaled residuals being less than 1.3 results in equal weighting. Scaling increases the residual magnitude causing de-weighting of larger residuals.

This manual tuning of the residual scale however is not desirable. One way to learn this scale directly is to let SRKO look for the  $c$  values that is smaller than 1, resulting in a tighter fit to the distribution. Notice changing the scale  $s$  is the same as changing the scale  $c$  in equation 3. Thus we implement a second version of SRKO, called SRKO\*, which can search through  $c$  values within the range  $[0.05 : 0.05 : 2]$ . The initialization point is kept the same at  $(\alpha, c) = (2, 1)$ . Figure 4 shows SRKO choosing the best  $\alpha$  and  $c$  with starting  $c = 1$  and a real set of residuals extracted during registration. Note how the negative log-likelihood decreases as a good fit for the residuals is found. This step is followed by optimization with the best  $\alpha$  and  $c$ . This learning-optimization cycle carries on until convergence.

Figures 5 and 6 show the parameters learned and the registration performance of SRKO\* for clean and noisy data. These figures show that SRKO\* is able to find low scale values close to 0.05 and give similar performance to scaled Huber and RKO thus removing the need for the manual tuning. SRKO\* performance for clean data registration is very close to scaled Huber, RKO, and FastReg. For the noisy case, SRKO\* performs worse for

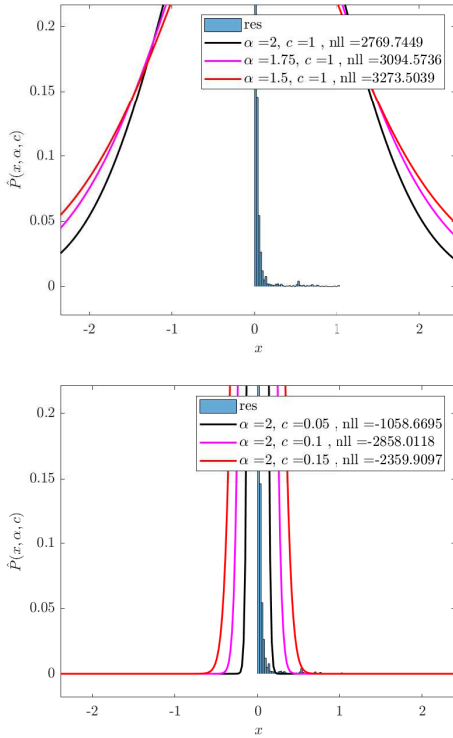


Fig. 4: Learning best fitting  $\alpha$  and  $c$  for SRKO\*

TABLE I: Average RMS errors over 25 clean data

methods	Huber	RKO	SRKO	FastReg	SRKO*
scale - 1	0.0123	0.0129	0.0120		
scale - 0.1	0.0080	0.0094	0.0090	0.0074	0.0073
scale - 0.05	0.0074	0.0074	0.0074		

3 out of 25 data sets, but maintains good performance for the rest. The reason for the larger errors could be due to SRKO\* not being able to learn the correct scale from the noisy data or because of it learning  $\alpha$  that is less robust than RKO (Fig 6). However, SRKO\* performs better than un-scaled RKO (scale-1) for both clean and noisy data. Another interesting aspect of the SRKO weights ( $\frac{\rho'(x, \alpha, c)}{x}$ ) is that they behave similar to Geman McClure weights [26] for very low values of  $c$  and  $\mu$  respectively (Fig. 7), i.e as  $c$  and  $\mu$  decreases, the peak weights start going down from 1.

TABLE II: Average RMS errors over 25 noisy data

methods	Huber	RKO	SRKO	FastReg	SRKO*
scale - 1	0.0532	0.0520	0.0496		
scale - 0.1	0.0287	0.0241	0.0282	0.0203	0.0320
scale - 0.05	0.0240	0.0166	0.0210		

For LIO-SAM implementations of RKO, we set the searchable  $\alpha$  range to be  $[-4 : 0.5 : 2]$ .  $c$  is fixed to 1. For SRKO\*,  $\alpha$  range is same and  $c$  range is  $[0.05, 0.1, 0.5, 0.75, 1.0, 1.25, 1.5, 1.75, 2.0]$ . Initializa-

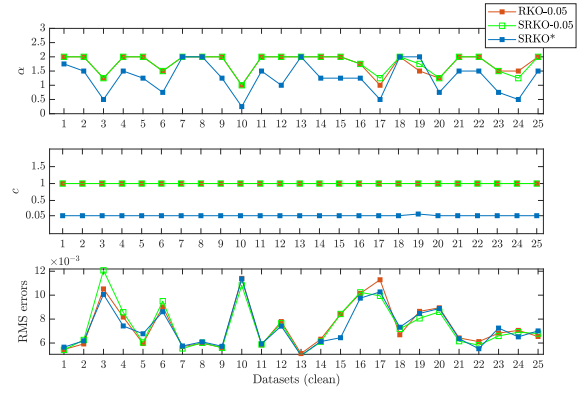


Fig. 5: Clean data results. Top: Learned  $\alpha$  values, Middle: Learned  $c$  values, Bottom: RMS errors normalized

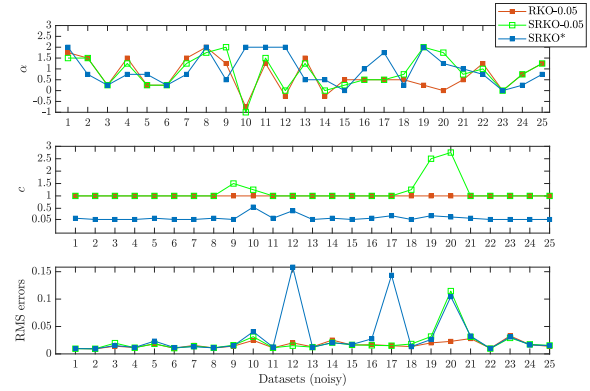


Fig. 6: Noisy data results. Top: Learned  $\alpha$  values, Middle: Learned  $c$  values, Bottom: RMS errors normalized

tion points for both are set to  $(\alpha, c) = (2, 1)$ . Here we chose smaller ranges of  $\alpha$  and  $c$  due to real-time running of LIO-SAM. FastReg is initialized with  $\mu = 20$  and Huber parameter is the same as the synthetic version. Table III shows the horizontal RMS errors of all methods with respect to standard LIO-SAM with loop closures. The performances of all methods were found to be similar to each other for *garden*, *rotation* and *campus(small)* data sets. SRKO\* is shown to outperform RKO by a larger margin for the *park* and *campus(large)* data sets. Figures 9, 10 show the learned parameters of RKO and

TABLE III: Horizontal RMS errors (m) w.r.t LIO-SAM+LC

methods	Huber	FastReg	RKO	SRKO*
<i>park</i>	0.58	0.70	0.89	0.68
<i>garden</i>	0.19	0.14	0.21	0.22
<i>rotation</i>	0.05	0.04	0.05	0.06
<i>campus(small)</i>	0.17	0.12	0.10	0.23
<i>campus(large)</i>	2.09	2.95	1.92	1.29

SRKO\* for *park* and *garden* data respectively. In the *park* data, RKO learns on the standard Gaussian, thus resulting in equal weighting throughout the trajectory. SRKO\* is able to learn non-Gaussian distributions, which

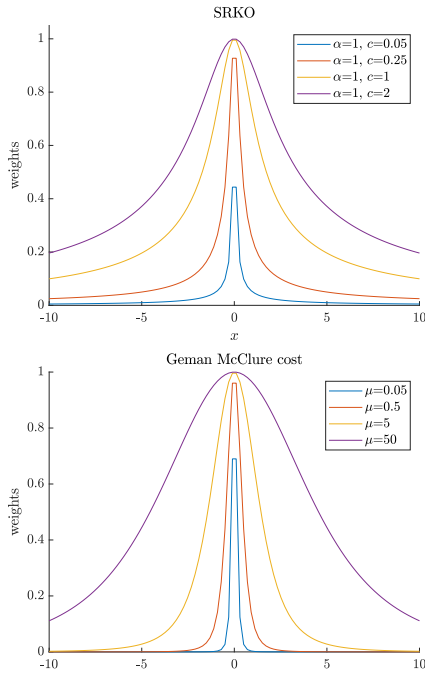


Fig. 7: Similarity between SRKO and Geman-McClure weights for low scale values

makes it more robust to outliers (Fig 8a, 8c). For the *garden* data, we see the same behaviour of RKO. Even though SRKO\* learns different  $c$  values, most of the  $\alpha$  values stay at 2. This results in very similar performance between RKO and SRKO\* for the *garden* case (Fig 8b) since  $\alpha = 2$  gives equal weighting to the residuals independent of the  $c$  values. Even though all learned  $c$  values were found to be less than or equal to 1, our algorithm can also learn values greater than 1.

## VIII. Conclusion and Future work

In this paper, we proposed to improve on RKO [2] by learning an additional scale parameter from the residuals. When considering the problem of single transformation point-cloud registration, with synthetic data, and lidar-inertial odometry, using real data, we showed that our version, SRKO\*, can learn a wider range of distributions than RKO, which makes it more robust to outliers. We also showed that if SRKO\* learns a Gaussian distribution ( $\alpha = 2$ ), then it converges to RKO independent of the  $c$  value. This is because all Gaussian distributions give equal weights to residuals following equation 2. The main disadvantage of these type of algorithms is the computational cost. Since both RKO and SRKO require learning of parameters from the current set residuals, they run slower than the standard LIO-SAM implementation. This forbids the use of larger parameter searching ranges for real-time computational tractability. Due to this computational cost of learning from a discrete range of parameter values, future work can focus on integrating the  $\alpha$  and  $c$  optimization in the IRLS framework.

## REFERENCES

- [1] J. N. Gross, C. Kilic, and T. E. Humphreys, “Maximum-likelihood power-distortion monitoring for gnss-signal authentication,” *IEEE Transactions on Aerospace and Electronic Systems*, vol. 55, no. 1, pp. 469–475, 2018.
- [2] N. Chebroul, T. Läbe, O. Vysotska, J. Behley, and C. Stachniss, “Adaptive robust kernels for non-linear least squares problems,” *IEEE Robotics and Automation Letters*, vol. 6, no. 2, pp. 2240–2247, 2021.
- [3] C. Kilic, N. Ohi, Y. Gu, and J. N. Gross, “Slip-based autonomous zupt through gaussian process to improve planetary rover localization,” *IEEE Robotics and Automation Letters*, vol. 6, no. 3, pp. 4782–4789, 2021.
- [4] J. Shi, H. Yang, and L. Carlone, “Robin: a graph-theoretic approach to reject outliers in robust estimation using invariants,” in *2021 IEEE International Conference on Robotics and Automation (ICRA)*. IEEE, 2021, pp. 13 820–13 827.
- [5] H. Yang, P. Antonante, V. Tzoumas, and L. Carlone, “Graduated non-convexity for robust spatial perception: From non-minimal solvers to global outlier rejection,” *IEEE Robotics and Automation Letters*, vol. 5, no. 2, pp. 1127–1134, 2020.
- [6] P. J. Huber, *Robust statistics*. John Wiley & Sons, 2004, vol. 523.
- [7] —, “John w. tukey’s contributions to robust statistics,” *Annals of statistics*, pp. 1640–1648, 2002.
- [8] F. R. Hampel, E. M. Ronchetti, P. J. Rousseeuw, and W. A. Stahel, *Robust statistics: the approach based on influence functions*. John Wiley & Sons, 2011, vol. 196.
- [9] M. Bosse, G. Agamennoni, I. Gilitschenski *et al.*, *Robust estimation and applications in robotics*. Now Publishers, 2016.
- [10] P. Babin, P. Giguere, and F. Pomerleau, “Analysis of robust functions for registration algorithms,” in *2019 International Conference on Robotics and Automation (ICRA)*. IEEE, 2019, pp. 1451–1457.
- [11] K. MacTavish and T. D. Barfoot, “At all costs: A comparison of robust cost functions for camera correspondence outliers,” in *2015 12th conference on computer and robot vision*. IEEE, 2015, pp. 62–69.
- [12] J. T. Barron, “A general and adaptive robust loss function,” in *Proceedings of the IEEE/CVF Conference on Computer Vision and Pattern Recognition*, 2019, pp. 4331–4339.
- [13] G. Agamennoni, P. Furgale, and R. Siegwart, “Self-tuning m-estimators,” in *2015 IEEE International Conference on Robotics and Automation (ICRA)*. IEEE, 2015, pp. 4628–4635.
- [14] M. J. Black and A. Rangarajan, “On the unification of line processes, outlier rejection, and robust statistics with applications in early vision,” *International journal of computer vision*, vol. 19, no. 1, pp. 57–91, 1996.
- [15] N. Sünderhauf and P. Protzel, “Switchable constraints for robust pose graph slam,” in *2012 IEEE/RSJ International Conference on Intelligent Robots and Systems*. IEEE, 2012, pp. 1879–1884.
- [16] P. Agarwal, G. D. Tipaldi, L. Spinello, C. Stachniss, and W. Burgard, “Robust map optimization using dynamic covariance scaling,” in *2013 IEEE International Conference on Robotics and Automation*. Ieee, 2013, pp. 62–69.
- [17] R. M. Watson and J. N. Gross, “Robust navigation in gnss degraded environment using graph optimization,” in *Proceedings of the 30th international technical meeting of the satellite division of the institute of navigation (ION GNSS+ 2017)*, 2017, pp. 2906–2918.
- [18] R. M. Watson, J. N. Gross, C. N. Taylor, and R. C. Leishman, “Enabling robust state estimation through measurement error covariance adaptation,” *IEEE Transactions on Aerospace and Electronic Systems*, vol. 56, no. 3, pp. 2026–2040, 2019.
- [19] —, “Robust incremental state estimation through covariance adaptation,” *IEEE Robotics and Automation Letters*, vol. 5, no. 2, pp. 3737–3744, 2020.
- [20] M. Ramezani, M. Mattamala, and M. Fallon, “Aeros: Adaptive robust least-squares for graph-based slam,” *Frontiers in Robotics and AI*, p. 23, 2022.

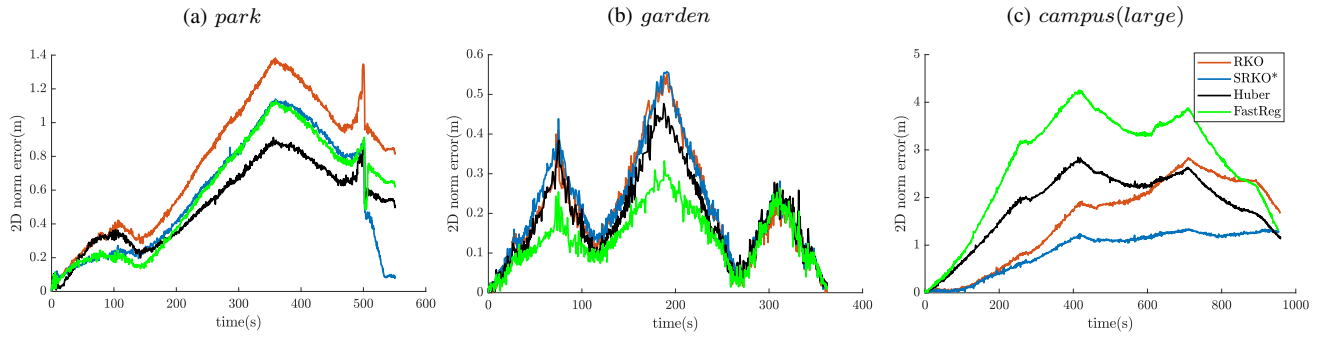


Fig. 8: 2D norm errors(m) for 3 data sets provided by [33]

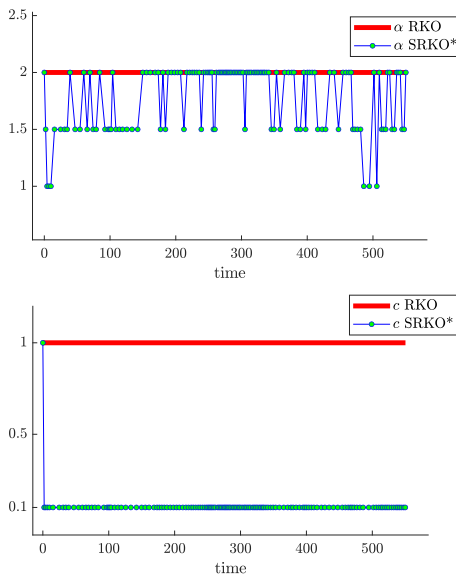


Fig. 9: Learned  $\alpha$  and  $c$  parameters for *park* data

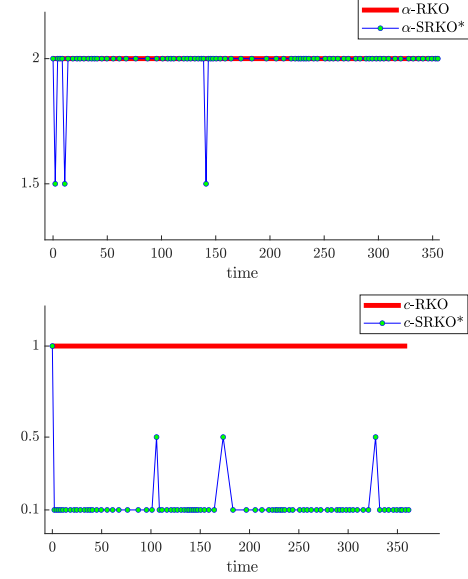


Fig. 10: Learned  $\alpha$  and  $c$  parameters for *garden* data

- [21] T.-J. Chin and D. Suter, "The maximum consensus problem: recent algorithmic advances," *Synthesis Lectures on Computer Vision*, vol. 7, no. 2, pp. 1–194, 2017.
- [22] M. A. Fischler and R. C. Bolles, "Random sample consensus: a paradigm for model fitting with applications to image analysis and automated cartography," *Communications of the ACM*, vol. 24, no. 6, pp. 381–395, 1981.
- [23] M. Zuliani, "Ransac for dummies," *Vision Research Lab, University of California, Santa Barbara*, 2009.
- [24] P. Antonante, V. Tzoumas, H. Yang, and L. Carlone, "Outlier-robust estimation: Hardness, minimally tuned algorithms, and applications," *IEEE Transactions on Robotics*, 2021.
- [25] J. G. Mangelson, D. Dominic, R. M. Eustice, and R. Vasudevan, "Pairwise consistent measurement set maximization for robust multi-robot map merging," in *2018 IEEE international conference on robotics and automation (ICRA)*. IEEE, 2018, pp. 2916–2923.
- [26] Q.-Y. Zhou, J. Park, and V. Koltun, "Fast global registration," in *European conference on computer vision*. Springer, 2016, pp. 766–782.
- [27] J. Behley and C. Stachniss, "Efficient surfel-based slam using 3d laser range data in urban environments," in *Robotics: Science and Systems*, vol. 2018, 2018, p. 59.
- [28] J.-E. Deschaud, P. Dellenbach, B. Jacquet, and F. Goulette, "Ct-icp: Real-time elastic lidar odometry with loop closure," 2021.
- [29] Y. Pan, P. Xiao, Y. He, Z. Shao, and Z. Li, "Mulls: Versatile lidar slam via multi-metric linear least square," in *2021 IEEE International Conference on Robotics and Automation (ICRA)*. IEEE, 2021, pp. 11 633–11 640.
- [30] K. Madsen, H. Nielsen, and O. Tingleff, "Methods for non-linear least squares problems (2nd ed.)," p. 60, 01 2004.
- [31] H. P. Gavin, "The levenberg-marquardt algorithm for nonlinear least squares curve-fitting problems," *Department of Civil and Environmental Engineering, Duke University*, pp. 1–19, 2019.
- [32] R. B. Rusu, N. Blodow, and M. Beetz, "Fast point feature histograms (fpfh) for 3d registration," in *2009 IEEE international conference on robotics and automation*. IEEE, 2009, pp. 3212–3217.
- [33] T. Shan, B. Englot, D. Meyers, W. Wang, C. Ratti, and D. Rus, "Lio-sam: Tightly-coupled lidar inertial odometry via smoothing and mapping," in *2020 IEEE/RSJ International Conference on Intelligent Robots and Systems (IROS)*. IEEE, 2020, pp. 5135–5142.